Available online at www.sciencedirect.com
ScienceDirect
Journal of Magnetic Resonance 188 (2007) 301–310
JMR Journal of Magnetic Resonance
www.elsevier.com/locate/jmr

A method for C^{α} direct-detection in *protonless* NMR

Wolfgang Bermel [a], Ivano Bertini [b,*], Isabella C. Felli [b], Manolis Matzapetakis [b,c], Roberta Pierattelli [b], Elizabeth C. Theil [c], Paola Turano [b]

[a] *Bruker BioSpin GmbH, Rheinstetten, Germany*
[b] *Magnetic Resonance Center and Department of Chemistry, University of Florence, Sesto Fiorentino, Italy*
[c] *CHORI (Childern's Hospital Oakland Research Institute) and Department of Nutritional Sciences and Toxicology, University of California, Berkeley, USA*

Received 8 June 2007; revised 5 July 2007
Available online 2 August 2007

Abstract

Attempts are made to efficiently decouple ^{13}C nuclei without significant loss of coherence during the application of the decoupling package. Such attempts are based on the S^3E spin-state selection method. A newly developed double S^3E (DS^3E) is particularly efficient for C^{α} detection for proteins as large as 480 kDa.

Keywords: Spin-state selection; Homonuclear decoupling; ^{13}C NMR; *Protonless* NMR; Protein assignment; Ferritin; Superoxide dismutase

1. Introduction

^{1}H direct-detection NMR experiments provide information for many complex biological macromolecules. However, the approach fails in other equally important systems such as large or paramagnetic proteins, parts of proteins affected by exchange processes or unfolded proteins. Therefore, a set of exclusively heteronuclear NMR experiments [1–3], named *protonless* NMR, has been developed with significant results [4–6].

Among the heteronuclei, ^{13}C direct-detection offers the best choice for its sensitivity and variety in proteins. Pioneering experiments by Markley in the 80s [7] were followed by a lag in favor of ^{1}H direct-detection methods. Recently, the application of ^{13}C direct-detection has shown its efficacy for paramagnetic systems [6,8–12], especially with the use of advanced hardware [1,13–15].

Backbone nuclei, C′ and C^{α}, give information on all the residues in a protein. Carbonyl detection is in general the best choice as the nucleus is coupled to only one other ^{13}C nucleus, simplifying the problem of homonuclear decoupling in the acquisition dimension. However, in large folded systems these nuclei display dramatic line broadening, particularly at high magnetic fields, due to the large chemical shift anisotropy (CSA). In unfolded systems, fast reorientational rates reduce the negative effects on linewidth due to CSA [5]. Alternatively, aliphatic nuclei would be the most useful for ^{13}C direct-detection in large proteins because of small CSA. Among aliphatic nuclei, C^{α} carbons are particularly attractive because they are part of the protein backbone thus providing information on protein conformation, and can be treated in a general way as their properties do not depend on the specific kind of amino acid. Since TROSY-like approaches have not yet been developed for backbone C^{α} H^{α} moiety, C^{α} direct-detection in ^{2}H labeled macromolecules is the most promising method for detection of these backbone nuclei in large systems.

Direct-detection of C^{α} is complicated by the presence of two large one-bond couplings with C′ and with C^{β} (except for glycines) that split the lines and reduce resolution. Thus, the efficiency of the methods to remove the coupling effect in the direct acquisition dimension is critical. Previously, we reported on the insertion of a double IPAP

* Corresponding author. Fax: +39 055 457 4271.
E-mail address: bertini@cerm.unifi.it (I. Bertini).

1090-7807/$ - see front matter © 2007 Elsevier Inc. All rights reserved.
doi:10.1016/j.jmr.2007.07.004

(DIPAP) filter to treat these couplings in selected pulse sequences [2,3]. However, the duration of the IPAP building-block is such that the sensitivity losses due to its insertion can be critical in fast relaxing systems. Other spin-state selection methods are available in the literature [16–23] and, among them, the S^3E [24] is particularly suited to be implemented in *protonless* pulse sequences.

We present here the results of the use of a double S^3E filter (DS^3E) tailored for C^α direct-detection in the analysis of monomeric superoxide dismutase, a 16 kDa protein, and of bullfrog ferritin M, a symmetric multimeric protein constituted by 24 four-helix bundle monomers for a total of 480 kDa. We present also another variant of the same filter optimized for C′ and methyl-detected experiments.

2. Experimental section

2.1. Samples preparation

The $^{13}C,^{15}N$ labeled cyclic peptide hymenistatin was used as a setup sample. A 20 mM sample was prepared in DMSO-d_6. All the spectra detailed below were recorded at 303 K.

The $^{13}C,^{15}N$ labeled monomeric mutant F50E/G51E/E133Q of superoxide dismutase was expressed and purified as previously reported [25]. The protein concentration in the final NMR sample was about 1.5 mM. The copper was reduced under anaerobic conditions with sodium ascorbate. The buffer was 20 mM phosphate at pH 5.0 and 10% D_2O was added for the lock signal. All the spectra detailed below were recorded at 298 K.

Bullfrog ferritin M was expressed in BL21 DE3 pLys *Escherichia coli* cells in $^{2}H,^{13}C,^{15}N$ labeled Spectra9 medium (Spectra Stable Isotopes) and purified as previously reported [26]. The purified protein was 90% deuterated, based on MALDI experiments. The protein concentration was 0.2 mM for the multimeric protein which equals 5 mM in monomer. The buffer was 20 mM phosphate at pH 7.5 and 10% D_2O was added for the lock signal. All the spectra detailed below were recorded at 308 K.

2.2. NMR experiments

The NMR experiments reported were recorded either on a 14.0 T Bruker AVANCE 600 spectrometer, operating at 600.13 MHz for ^1H and 150.91 MHz for ^{13}C or on a 16.4 T Bruker AVANCE 700 spectrometer, operating at 700.13 MHz for ^1H and 176.08 MHz for ^{13}C. The 600 MHz NMR spectrometer was equipped with a standard triple-resonance (TXI) probe. On the 16.4 T NMR spectrometer two probes were used: a triple-resonance probe optimized for ^{13}C sensitivity (TXO, S/N 500:1, on the ASTM standard sample) and a new generation cryogenically cooled probe optimized for ^{13}C sensitivity (TCI, S/N 1500:1, on the ASTM standard sample) as well as for ^1H sensitivity.

The experiments on the $^{13}C,^{15}N$ labeled cyclic octapeptide hymenistatin, were acquired on the 14.0 T NMR spectrometer. The ^1H, ^{13}C and ^{15}N carrier frequencies were placed at 4.7, 53.5 and 115.5 ppm, respectively, and ^{13}C pulses were given at 173, 53.5 and 43.17 ppm to excite or invert C′, C^α and $C^{\alpha/\beta}$ spins, respectively. Composite pulse decoupling was applied during acquisition and during some of the elements of the pulse sequence with RF field strength of 3.5 and 1.1 kHz for ^1H (waltz-16) [27] and ^{15}N (garp-4) [28], respectively. For ^{13}C the following pulses were used: 320 μs with Q5 (and time reversed Q5) shapes [29] for C^α, C^{ali} excitation, 256 μs Q3 shape and 1 ms Q3 shape [29] for C'/C^{ali} and C^α inversion, respectively. Experiments were acquired with a relaxation delay of 1.5 s and with an acquisition times of 170 ms (2048 data points) and with 256 scans per increment. The spectral width was 39 ppm (C^α direct-detection).

The 2D C^α-TOCSY-DIPAP and 2D C^α-TOCSY-DS^3E experiments on monomeric ^{13}C, ^{15}N labeled SOD were acquired on the 16.4 T NMR spectrometer with the TXO probe. The ^1H, ^{13}C and ^{15}N carrier frequencies were placed at 3.5, 55 and 120.0 ppm, respectively, and ^{13}C pulses were given at 175, 55 and 39 ppm to excite or invert C′, C^α and $C^{\alpha/\beta}$ spins, respectively. For ^{13}C the following pulses were used: 274 μs with Q5 (and time reversed Q5) shapes [29] for C^α, C^{ali} excitation, 220 μs Q3 shape and 860 ms Q3 shape [29] for C'/C^{ali} and C^α inversion, respectively. The FLOPSY [30] spin-lock was 12 ms long with an RF field strength of 10 kHz. Composite pulse decoupling was applied during acquisition and during some of the elements of the pulse sequence with RF field strength of 1.6 and 0.625 kHz for ^1H (waltz-16) [27] and ^{15}N (garp-4) [28]. Experiments were acquired with a relaxation delay of 1.5 s and with an acquisition time of 110 ms and with 128 scans per increment. Spectral widths of 100×100 ppm were used (2048×320 data points).

The 2D NOESY and 2D C^α-NOESY-DS^3E experiments on ^{13}C, ^{15}N, 90% ^2H labeled ferritin were acquired on the 16.4 T NMR spectrometer with the TCI probe. The ^1H, ^2H ^{13}C and ^{15}N carrier frequencies were placed at 3.5, 55 and 120.0 ppm, respectively, and ^{13}C pulses were given at 175, 55 and 39 ppm to excite or invert C′, C^α and $C^{\alpha/\beta}$ spins, respectively. For ^{13}C the following pulses were used: 274 μs with Q5 (and time reversed Q5) shapes [29] for C^α, C^{ali} excitation, 220 μs Q3 shape and 860 ms Q3 shape [29] for C'/C^{ali} and C^α inversion, respectively. The 1D spin-echo experiments on C^α were acquired with a 860 μs Q3 shape π pulse in the middle of the echo times reported in Fig. 5. Composite pulse decoupling was applied during acquisition and during some of the elements of the pulse sequence with RF field strength of 1.6, 1.0 and 1.0 kHz for ^1H (waltz-16) [27], ^2H (waltz-16) [27] and ^{15}N (garp-4) [28]. Decoupling of ^{15}N was switched off during acquisition. Experiments were acquired with a mixing time of 500 ms, a relaxation delay of 2.5 s and with an acquisition time of 45 ms. Spectral widths of 127×127 ppm were used. The 2D C^α-NOESY-DS^3E was acquired with 96 scans per increment

and with $2048 \times 512 \times 4$ data points; the 2D NOESY was acquired with 48 scans per increment and with 2048×512 data points.

The 2D Methyl-NOESY-S^{3}E experiment on ^{13}C, ^{15}N, 90% 2H labeled ferritin was acquired on the 16.4 T NMR spectrometer with the TCI cryoprobe in the same conditions as the other NOESY experiments on ferritin except for the following parameters. The ^{13}C carrier was placed at 11 ppm and ^{13}C pulses were given at 11 and 35 ppm to excite or invert CMe and C$^\alpha$ spins, respectively. For ^{13}C the following pulses were used: 310 μs with Q5 (and time reversed Q5) shapes [29] for C^{Me} excitation, 860 and 400 μs for C^{Me} and C$^\alpha$ inversion, respectively. The experiment was acquired with an acquisition time of 86 ms, a spectral width of 100×100 ppm, 96 scans per increment and $3072 \times 256 \times 4$ data points.

For experiments that employ the IPAP block [3,31] in the acquisition dimension, for each time increment in the indirect dimension two FIDs were separately stored, one for the anti-phase and one for the in-phase components. The two FIDs were then added and subtracted to separate the two multiplet components. These were then shifted to the center of the original multiplet (by $J_{C'C^\alpha}/2$ Hz) and again added to obtain a singlet. In experiments that employ the DIPAP block [2,3], for each time increment in the indirect dimension, four FIDs were separately stored, and the resulting sub-matrices were added and subtracted in pairs to separate the four multiplet components, then shifted by $(\pm J_{C'C^\alpha}/2)$ and $(J_{C^\alpha C^\beta}/2$ Hz) and summed again to obtain a singlet.

In the experiments that employ the S^{3}E block [3,32], for each time increment in the indirect dimension two FIDs were separately stored. These were summed and subtracted to separate the two multiplet components and one of the two was phase-shifted by 90°. These were then shifted to the center of the original multiplet (by $J_{C'C^\alpha}/2$ Hz) and again summed to obtain a singlet. For experiments that employ the DS^{3}E block, four different linear combinations of the four FIDs stored separately (two need to be phase-shifted by π/2) give the four separated multiplet components. Each of the four multiplet components were shifted by $(\pm J_{C'C^\alpha}/2$ Hz) and $(\pm J_{C^\alpha C^\beta}/2$ Hz) to the center of the original multiplet in order to suppress the C$^\alpha$–C as well as the C$^\alpha$–C$^\beta$ coupling and summed again to obtain a singlet.

The new NOESY pulse sequences (C$^\alpha$-NOESY-DS^{3}E and Methyl-NOESY-S^{3}E) are described in detail in the Appendix.

3. Description of the pulse sequences

3.1. The DS^{3}E building-block

The DS^{3}E block for direct-detection of C$^\alpha$ is reported in Fig. 1.

The delays a, b and c are set to allow for the evolution of the one-bond C$^\alpha$–C′ and C$^\alpha$–C$^\beta$ couplings for a total evolution time of $1/4J$ each ($a + b + c = 1/4J_{C^\alpha C^\beta}$ and $a - b + c = 1/4J_{C'C^\alpha}$, with $a + b = c$). The minimal duration of the block is determined by the smaller coupling that needs to be suppressed ($J_{C^\alpha C^\beta}$). In all cases the central pulse inverts both the C$^\alpha$ and C$^\beta$ spins to allow evolution of the C$^\alpha$–C$^\beta$ coupling for the whole duration of the building-block. The four experiments therefore differ in the position of the π pulses on C′ (these are always applied in pairs to compensate for Bloch–Siegert shifts) and on C$^\alpha$. The effect of the π pulses is different if the pulses are applied right after creation of C$^\alpha$ transverse magnetization or at the end of the block after evolution of the two scalar couplings, when actually the four operators related to the different multiplet components are simultaneously present. Therefore the change in position of the C′ and C$^\alpha$ π pulses allows us to manipulate the signs of the four operators in order to be able to obtain the suitable linear combinations required for the separation of the four multiplet components (Fig. 2). A detailed description of the DS^{3}E building-block through product operators is reported in the Appendix.

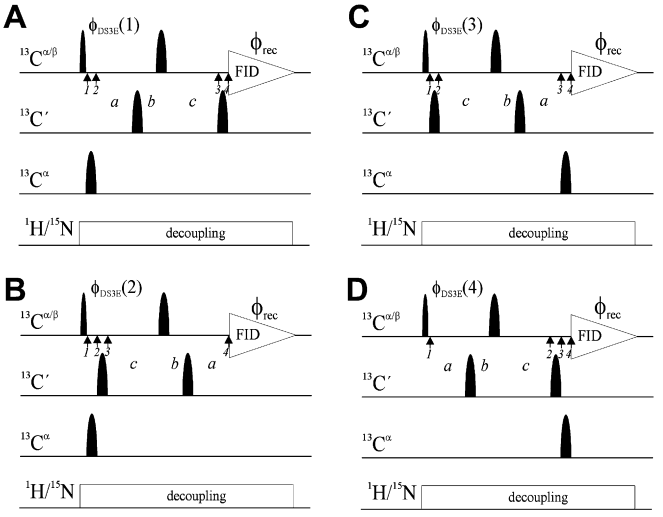

Fig. 1. The 1D version of the DS^{3}E building-block for direct-detection of C$^\alpha$. Narrow and wide black vertical symbols indicate band-selective π/2 and π pulses, respectively. The four variants of the 1D experiment that are necessary to separate, through linear combinations, the four components of the C$^\alpha$ multiplet are reported in panels A–D. The delays a, b and c are set to allow for the evolution of the one-bond C$^\alpha$–C and C$^\alpha$–C$^\beta$ couplings for a total evolution time of $1/4J$ each ($a + b + c = 1/4J_{C^\alpha C^\beta} = 7.2$ ms and $a - b + c = 1/4J_{C^\alpha - C'} = 4.5$ ms, with $a + b = c$). All the pulses, unless explicitly indicated, have phase x. The minimal phase cycles are: $\phi_{DS^3E}(1) = x, -x$, $\phi_{DS^3E}(2) = y, -y$, $\phi_{DS^3E}(3) = -y, y$, $\phi_{DS^3E}(4) = x, -x$, $\phi_{rec} = x, -x$. If the molecule is ^{2}H labeled, ^{2}H decoupling should be activated in parallel to ^{1}H decoupling (or in alternative to ^{1}H decoupling, depending on the extent of ^{2}H isotopic enrichment).

3.2. The S^{3}E building-block

The S^{3}E block for direct-detection of methyl groups of alanine residues is shown in Fig. 3. In the original paper

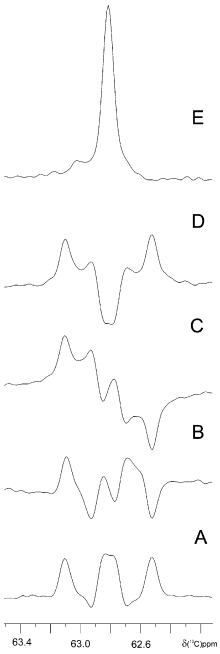

Fig. 2. The four different 1D experiments, acquired with the pulse sequence reported in Fig. 1 (panels A–D) on ^{13}C, ^{15}N labeled cyclic octapeptide hymenistatin (C^{α} of Pro 5), are reported from bottom to top (A–D). The 1D spectrum after appropriate linear combination, phase shift and frequency shift of each component to the center of the multiplet is reported on top (panel E). This is scaled to the single traces in order to have the same noise intensity.

[16] as well as in our previous application of the method to C′ direct-detection [2,32], two π/2 pulses were used to achieve a 0 or π effective rotation necessary to manipulate the relative signs of the different operators in the two independent experiments needed to separate the different multiplet components. They are replaced by a single π pulse that is positioned either at the end or at the beginning of the S^3E block, along the same idea used for the double S^3E block proposed here for C^{α} direct-detection. The pulse sequence looks similar to the IPAP scheme but while in the IPAP filter the transverse coherence that is created after the first π/2 pulse is allowed to evolve under the effect of the relevant scalar coupling for $1/2J$ in order to be completely converted into anti-phase magnetization, in the S^3E approach this delay is reduced by a factor of 2 in order to detect a linear combination of in-phase and anti-phase components. In the current version of the S^3E block both components are obtained by using π pulses on the spins in the plane right after creation of transverse coherence or right before acquisition in order to change the sign of one of the two components in alternate experiments. This approach improves the performance of the S^3E element, not only for methyl groups of alanine residues but also for direct-detection of carbonyls. In this case the pulses indicated with $^{13}C^{Me}$ should be band-selective pulses on $^{13}C'$, and the delay a should be optimized to $1/8J_{C^{\alpha}-C'}$ ($2a = 4.5$ ms). A detailed description of the S^3E building-block through product operators is reported in the Appendix.

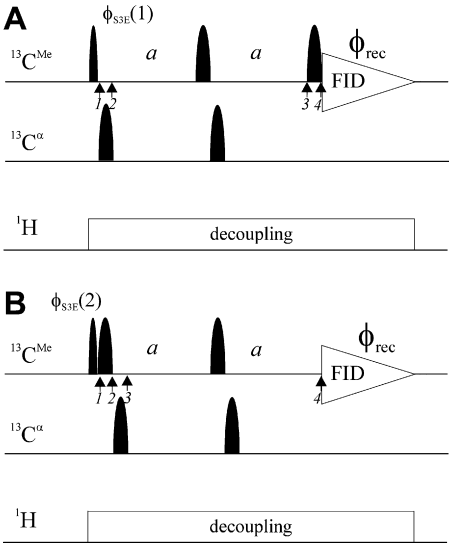

Fig. 3. The 1D version of the S^3E building-block for direct-detection of alanine methyl carbons. Narrow and wide vertical symbols indicate band-selective π/2 and π pulses, respectively. The two variants of the 1D experiment that are necessary to separate, through linear combinations, the two components of the C^{β} multiplet in alanine residues are reported in panels (A and B). The delay a is set to allow for the evolution of the one-bond C^{α}–C^{β} coupling for a total evolution time of $1/4J_{C^{\alpha}C^{\beta}} = 7.2$ ms ($2a = 7.2$ ms). All the pulses, unless explicitly indicated, have phase x. The phase cycles are: $\phi_{S^3E}(1) = x, -x,\ \phi_{S^3E}(2) = y, -y,\ \phi_{rec} = x,\ -x$. This experimental approach can be applied also to remove the C^{α}–C′ coupling in experiments based on C′ direct-detection. The pulses indicated with $^{13}C^{Me}$ should be band-selective pulses on $^{13}C'$, the delay $2a$ should be optimized to $1/4J_{C^{\alpha}-C'}$ and ^{15}N decoupling should be switched on in parallel to ^{1}H decoupling. If the molecule is ^{2}H labeled, ^{2}H decoupling should be activated in parallel to ^{1}H decoupling (or in alternative to ^{1}H decoupling, depending on the extent of ^{2}H isotopic enrichment).

4. Results and discussion

The insertion of the DS^3E building-block in selected experiments for direct-detection of C^{α} is tested on molecules with different molecular mass to verify the performance in terms of removing the large one-bond carbon–carbon scalar couplings involving C^{α} spins and to evaluate the effect of transverse relaxation in comparison with other spin-state selective schemes that have been recently proposed for this task [2,32]. The present scheme minimizes the time in which ^{13}C magnetization is transverse and is thus *relaxation optimized*.

The set-up of the DS^3E building-block was performed on the ^{13}C, ^{15}N labeled cyclic octapeptide hymenistatin. The four components of the NMR signal acquired separately as well as after the appropriate data handling show that the large one-bond C′–C^{α} as well as the C^{α}–C^{β} couplings are largely suppressed (Fig. 2).

The DS^3E building-block was then inserted at the end of the TOCSY experiment (C^{α}-TOCSY-DS^3E) and compared with the analogous experiment that employs the DIPAP block to suppress the large one-bond C^{α} carbon–carbon couplings (C^{α}-TOCSY-DIPAP) [2]. These experiments were recorded on monomeric ^{13}C, ^{15}N labeled reduced

superoxide dismutase [33]. Inspection of the 2D maps (Fig. 4) shows that the large one-bond C^{α} carbon–carbon couplings have been suppressed in a very similar way in the two versions of the experiment. The number of observed correlations is comparable in the two spectra acquired under the same conditions, with a number of cross peaks out of the noise only in the DS^3E version of the experiment. Measuring the intensity for a few well isolated cross peaks shows that already with the moderate molecular mass of monomeric superoxide dismutase (16 kDa) the effect of relaxation is sizable and, on average, the cross peak intensities are larger by a factor between 1.1 and 1.3 in the DS^3E version of the experiments.

With the increase in molecular mass, the increase in cross relaxation rates and the decrease in longitudinal rates make the NOESY-transfer based experiments the preferred choice for the assignment of a protein [26,34,35]. In fact the effect of spin diffusion in large molecules becomes so efficient that NOESY experiments can be actively exploited to identify directly bound carbon spins [26,31]. So, NOESY experiments yield spin system information similar to that conventionally obtained from TOCSY experiments [26,31]. The DS^3E block was thus included in the NOESY experiment (C^{α}-NOESY-DS^3E, see Appendix A.3) and applied to ^{13}C, ^{15}N, 90%^{2}H labeled bullfrog ferritin M with the aim of improving the resolution of particularly crowded regions of the spectrum.

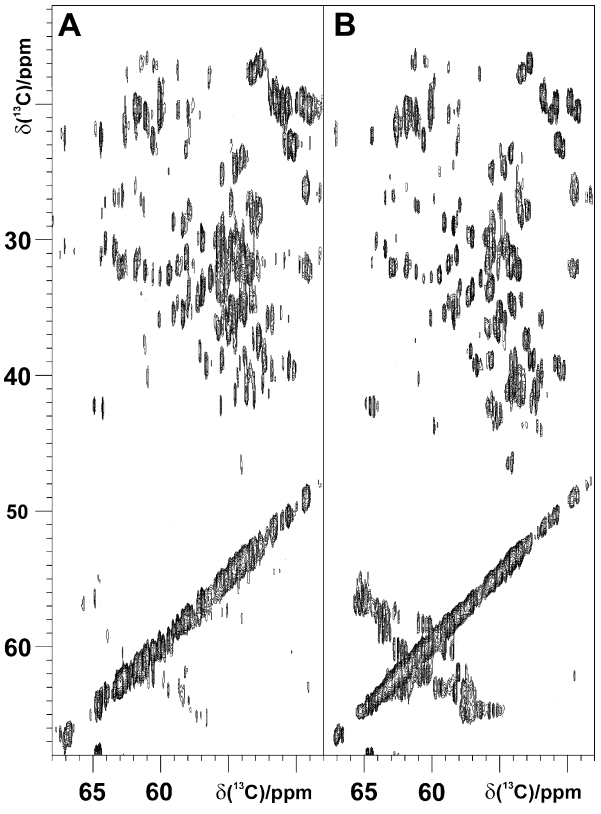

Fig. 4. The (A) 2D C^{α} TOCSY-DIPAP and the (B) 2D C^{α} TOCSY-DS^3E experiments acquired at 16.4 T on monomeric ^{13}C, ^{15}N labeled reduced superoxide dismutase under similar experimental conditions. The number of observed correlations is comparable in the two spectra with a few cross peaks out of the noise only in the DS^3E version of the experiment. In case of threonine or serines the one-bond coupling suppression works well for the C^{α}–C' coupling but is compromised for the C^{α}–C^{β} coupling, as the latter nuclei resonate in the same spectral region, and the signals are poorly decoupled.

A check on the transverse relaxation rates of C^{α} spins in ferritin clearly shows that relaxation losses that would arise from the 14 ms necessary for the DIPAP block are sizable (Fig. 5) and for this reason no attempt was made to record the C^{α}-NOESY-DIPAP version of the experiment on ferritin. A reference NOESY experiment without any spin-state selection was instead acquired for comparison (Fig. 6A). A first glimpse on the 2D maps shows a great improvement in resolution for the 2D C^{α}-NOESY-DS^3E (Fig. 6B).

A count of the cross peaks in the C^{α}–C^{ali} region of the 2D C^{α}-NOESY-DS^3E experiment allows us to recognize 160 resolved peaks. Out of these, 56 peaks were severely overlapped in the NOESY without any spin-state selection and could only be resolved in the DS^3E version of the experiment. The increased resolution (see the insets in Fig. 6 as an example) of the C^{α}-NOESY-DS^3E spectrum permits the extension of the assignment of some residues. For example, while the C^{β} to aromatic cross peaks attributable to two patterns of Tyr could be detected in the NOESY without spin-state selection, the patterns for 6 Tyr, including the C^{α}–C^{β} connectivities, can be clearly observed in the C^{α}-NOESY-DS^3E experiment. In the latter experiment it is also possible to resolve the cross peaks of the two Cys, and to observe the previously unresolved C^{α}s of four Glu/Gln and three Asp/Asn. An additional C^{α} of a His residue is also detectable. On the other hand, a dozen of well isolated peaks, that were weak in the NOESY experiment, are missing in the DS^3E version because of an attenuation of the signal due to the inclusion of the DS^3E block in the experiment.

Fig. 7 (A and C) shows a zoom in the region containing the C^{α}–C^{β} correlations of alanine residues as an instructive example of the increased resolution obtained for ferritin

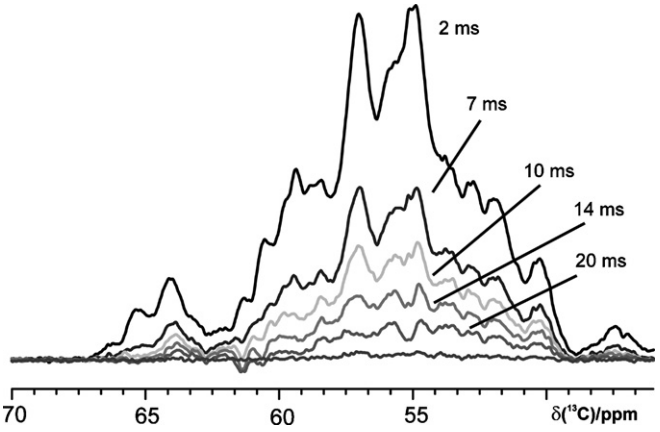

Fig. 5. 16.4 T ^{13}C 1D spin-echo experiments on the C^{α} region of ferritin M acquired at 308 K. The duration of the spin-echo is reported in the figure. Band-selective π pulses on C^{α} were used.

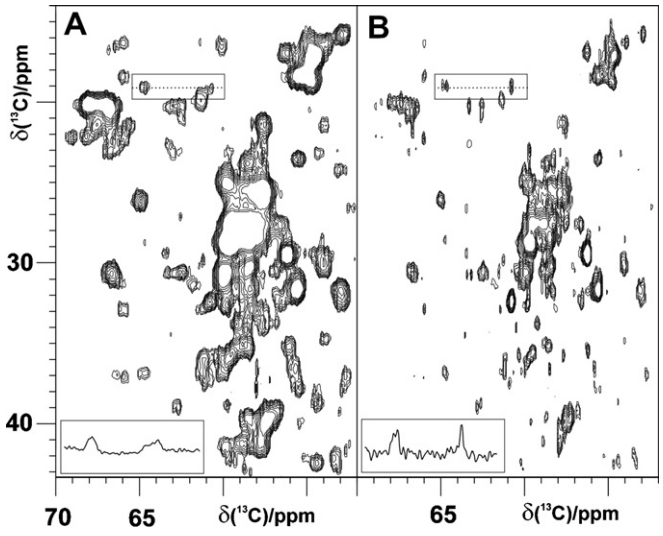

Fig. 6. 16.4 T (A) 2D ^{13}C-NOESY and (B) 2D C$^{\alpha}$-NOESY-DS^{3}E experiments acquired on bullfrog ferritin M. The traces in the insets are the 1D sections of the portion of rows indicated by dashed lines in the two panels.

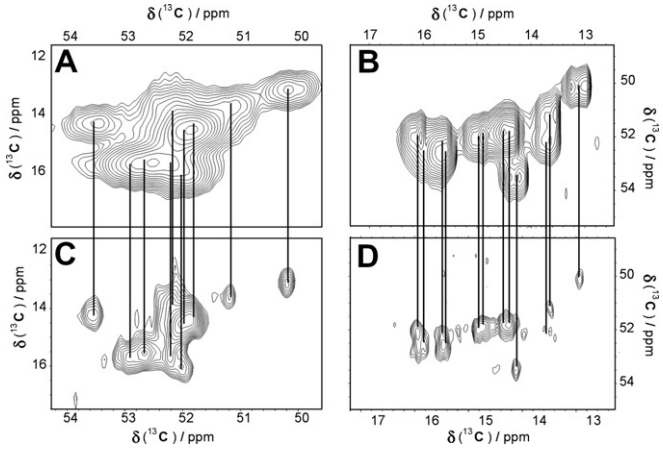

Fig. 7. Top panels: zoom on the symmetric regions of the ^{13}C NOESY spectrum reported in Fig. 6A containing the (A) C$^{\alpha}$ (ω_2 direct dimension) $-$C$^{\beta}$ (ω_1 indirect dimension) and (B) C$^{\beta}$ (ω_2, direct dimension) $-$C$^{\alpha}$ (ω_1, indirect dimension) correlations of alanine residues. Bottom panels: zoom on the same regions extracted from (C) the C$^{\alpha}$-NOESY-DS^{3}E spectrum reported in Fig. 6B and from (D) the Methyl-NOESY-S^{3}E spectrum.

with the C$^{\alpha}$-NOESY-DS^{3}E experiment (Fig. 7C). Indeed, it can be noted that the DS^{3}E-based decoupling actually allows us to clearly identify 10 correlations out of the 12 Ala residues present. Improvement in resolution is consistent with an efficient suppression of the relevant C–C couplings and, even at the expense of sensitivity, this experiment is key to resolve ambiguities such as those in the alanine region.

Correlations to the methyl groups could also be observed by direct-detection of methyl carbons rather than of the C$^{\alpha}$ (symmetric part of the spectrum). In order to remove the large C$^{\alpha}$–C$^{\beta}$ coupling we designed a building-block tailored to detect methyl groups of alanine residues removing the large one-bond coupling in the direct acquisition dimension (Fig. 3), that has been included in the NOESY experiment (Methyl-NOESY-S^{3}E, see Appendix A.4). The result is reported in Fig. 7D. The combination of the two spectra actually allows us to identify all the correlations deriving from the 12 alanines present in ferritin.

5. Conclusions

Concluding, the DS^{3}E building-block effectively reduces the time in which transverse relaxation is operative by a factor of 2 compared to the DIPAP, and it is used successfully for the study of the ^{13}C,^{15}N labeled, monomeric superoxide dismutase, with a mass of 16 kDa. For a ^{13}C,^{15}N,^{2}H labeled 480 kDa protein like ferritin, the use of the DS^{3}E is the only choice to increase resolution.

Furthermore, the new variant of the S^{3}E building-block, with improved performance compared to the original version, was applied to the detection of the methyl carbons of alanine residues in ferritin, and it may be useful in general for the identification of methyl resonances in case of fully deuterated alanines, that are not "reprotonated" with the methyl reprotonation strategy [36].

The novel results obtained with ferritin protein nanocages demonstrate that ^{13}C direct-detection NMR is a crucial strategy for the study of proteins larger than 40 kDa and, most importantly, for the study of protein–protein interactions.

Acknowledgments

Dr. O. Mechnich and Prof. H. Kessler are gratefully acknowledged for providing the ^{13}C,^{15}N labeled cyclic octapeptide hymenistatin. Support from the EUNMR-JRA project contract # RII3-026145, the SPINE2-COMPLEXES project contract # 031220, the MIUR PRIN-2005 2005039878 Grant and the NIH Grant # DK20251 is gratefully acknowledged.

Appendix A

A.1. The DS^{3}E building-block

Let's consider a spin system constituted by three spins, C$^{\alpha}$, C$'$ and C$^{\beta}$, where, C$^{\alpha}$ is coupled to C$^{\beta}$, through $J_{C\alpha C\beta}$ and to C$'$ through $J_{C'C^{\alpha}}$. The evolution of product operators for the 4 different experiments shown in Fig. 1 at the different time points (indicated in Fig. 1 with numbers in italic) is reported hereafter:

Panel A

(1) $-C^{\alpha}_{y}$

$1 \rightarrow 2$ π_x pulse on C$^{\alpha}$ spin

(2) $+C^{\alpha}_{y}$

$2 \rightarrow 4$

evolution of the C^{α}–C^{β} scalar coupling for $1/4J_{C^{\alpha}C^{\beta}}$ and of the C^{α}–C' scalar coupling for $1/4J_{C'C^{\alpha}}$, refocusing of C^{α} chemical shift (change is sign of the original $+C^{\alpha}_{y}$ operator due to the central π_x pulse on C^{α} spins) and final π_x pulse on C' spins ($3 \rightarrow 4$).

$$
\begin{aligned}
(4)\ & -C^{\alpha}_{y}\cos(\pi J_{C'C^{\alpha}}2a)\cos(\pi J_{C^{\alpha}C^{\beta}}(2c))\\
& -2C^{\alpha}_{x}C'_{z}\sin(\pi J_{C'C^{\alpha}}2a)\cos(\pi J_{C^{\alpha}C^{\beta}}(2c))\\
& +2C^{\alpha}_{x}C^{\beta}_{z}\cos(\pi J_{C'C^{\alpha}}2a)\sin(\pi J_{C^{\alpha}C^{\beta}}(2c))\\
& -4C^{\alpha}_{y}C'_{z}C^{\beta}_{z}\sin(\pi J_{C'C^{\alpha}}2a)\sin(\pi J_{C^{\alpha}C^{\beta}}(2c))
\end{aligned}
$$

Panel B

$$(1)\ +C^{\alpha}_{x}$$

$1 \rightarrow 2$ π_x pulse on C^{α} spin

$$(2)\ +C^{\alpha}_{x}$$

$2 \rightarrow 4$

initial π_x pulse on C' spin ($2 \rightarrow 3$); evolution of the C^{α}–C^{β} scalar coupling for $1/4\ J_{C^{\alpha}C^{\beta}}$ and of the C^{α}–C' scalar coupling for $1/4J_{C'C^{\alpha}}$, refocusing of C^{α} chemical shift (the sign of the original $+\ C^{\alpha}_{x}$ operator due to the central π_x pulse on C^{α} spin does not change).

$$
\begin{aligned}
(4)\ & +C^{\alpha}_{x}\cos(\pi J_{C'C^{\alpha}}2a)\cos(\pi J_{C^{\alpha}C^{\beta}}(2c))\\
& +2C^{\alpha}_{y}C'_{z}\sin(\pi J_{C'C^{\alpha}}2a)\cos(\pi J_{C^{\alpha}C^{\beta}}(2c))\\
& +2C^{\alpha}_{y}C^{\beta}_{z}\cos(\pi J_{C'C^{\alpha}}2a)\sin(\pi J_{C^{\alpha}C^{\beta}}(2c))\\
& -4C^{\alpha}_{x}C'_{z}C^{\beta}_{z}\sin(\pi J_{C'C^{\alpha}}2a)\sin(\pi J_{C^{\alpha}C^{\beta}}(2c))
\end{aligned}
$$

Panel C

$$(1)\ -C^{\alpha}_{x}$$

$1 \rightarrow 3$

initial π_x pulse on C' spin ($2 \rightarrow 3$); evolution of the C^{α}–C^{β} scalar coupling for $1/4J_{C^{\alpha}C^{\beta}}$ and of the C^{α}–C' scalar coupling for $1/4J_{C'C^{\alpha}}$, refocusing of C^{α} chemical shift (the sign of the original $-C^{\alpha}_{x}$ operator due to the central π_x pulse on C^{α} spin does not change).

$$
\begin{aligned}
(3)\ & -C^{\alpha}_{x}\cos(\pi J_{C'C^{\alpha}}2a)\cos(\pi J_{C^{\alpha}C^{\beta}}(2c))\\
& -2C^{\alpha}_{y}C'_{z}\sin(\pi J_{C'C^{\alpha}}2a)\cos(\pi J_{C^{\alpha}C^{\beta}}(2c))\\
& -2C^{\alpha}_{y}C^{\beta}_{z}\cos(\pi J_{C'C^{\alpha}}2a)\sin(\pi J_{C^{\alpha}C^{\beta}}(2c))\\
& +4C^{\alpha}_{x}C'_{z}C^{\beta}_{z}\sin(\pi J_{C'C^{\alpha}}2a)\sin(\pi J_{C^{\alpha}C^{\beta}}(2c))
\end{aligned}
$$

$3 \rightarrow 4$ π_x pulse on C^{α} spin

$$
\begin{aligned}
(4)\ & -C^{\alpha}_{x}\cos(\pi J_{C'C^{\alpha}}2a)\cos(\pi J_{C^{\alpha}C^{\beta}}(2c))\\
& +2C^{\alpha}_{y}C'_{z}\sin(\pi J_{C'C^{\alpha}}2a)\cos(\pi J_{C^{\alpha}C^{\beta}}(2c))\\
& +2C^{\alpha}_{y}C^{\beta}_{z}\cos(\pi J_{C'C^{\alpha}}2a)\sin(\pi J_{C^{\alpha}C^{\beta}}(2c))\\
& +4C^{\alpha}_{x}C'_{z}C^{\beta}_{z}\sin(\pi J_{C'C^{\alpha}}2a)\sin(\pi J_{C^{\alpha}C^{\beta}}(2c))
\end{aligned}
$$

Panel D

$$(1)\ -C^{\alpha}_{y}$$

$1 \rightarrow 3$

evolution of the C^{α}–C^{β} scalar coupling for $1/4J_{C^{\alpha}C^{\beta}}$ and of the C^{α}–C' scalar coupling for $1/4J_{C'C^{\alpha}}$, refocusing of C^{α} chemical shift (change is sign of the original $+C^{\alpha}_{y}$ operator due to the central π_x pulse on C^{α} spin) and final π_x pulse on C' spin ($2 \rightarrow 3$).

$$
\begin{aligned}
(3)\ & +C^{\alpha}_{y}\cos(\pi J_{C'C^{\alpha}}2a)\cos(\pi J_{C^{\alpha}C^{\beta}}(2c))\\
& +2C^{\alpha}_{x}C'_{z}\sin(\pi J_{C'C^{\alpha}}2a)\cos(\pi J_{C^{\alpha}C^{\beta}}(2c))\\
& -2C^{\alpha}_{x}C^{\beta}_{z}\cos(\pi J_{C'C^{\alpha}}2a)\sin(\pi J_{C^{\alpha}C^{\beta}}(2c))\\
& +4C^{\alpha}_{y}C'_{z}C^{\beta}_{z}\sin(\pi J_{C'C^{\alpha}}2a)\sin(\pi J_{C^{\alpha}C^{\beta}}(2c))
\end{aligned}
$$

$3 \rightarrow 4$ π_x pulse on C^{α} spin

$$
\begin{aligned}
(4)\ & -C^{\alpha}_{y}\cos(\pi J_{C'C^{\alpha}}2a)\cos(\pi J_{C^{\alpha}C^{\beta}}(2c))\\
& +2C^{\alpha}_{x}C'_{z}\sin(\pi J_{C'C^{\alpha}}2a)\cos(\pi J_{C^{\alpha}C^{\beta}}(2c))\\
& -2C^{\alpha}_{x}C^{\beta}_{z}\cos(\pi J_{C'C^{\alpha}}2a)\sin(\pi J_{C^{\alpha}C^{\beta}}(2c))\\
& -4C^{\alpha}_{y}C'_{z}C^{\beta}_{z}\sin(\pi J_{C'C^{\alpha}}2a)\sin(\pi J_{C^{\alpha}C^{\beta}}(2c))
\end{aligned}
$$

Summarizing:

Panel A	$-C^{\alpha}_{y}$	$-2C^{\alpha}_{x}C'_{z}$	$+2C^{\alpha}_{x}C^{\beta}_{z}$	$-4C^{\alpha}_{y}C'_{z}C^{\beta}_{z}$
Panel B	$+C^{\alpha}_{x}$	$+2C^{\alpha}_{y}C'_{z}$	$+2C^{\alpha}_{y}C^{\beta}_{z}$	$-4C^{\alpha}_{x}C'_{z}C^{\beta}_{z}$
Panel C	$-C^{\alpha}_{x}$	$+2C^{\alpha}_{y}C'_{z}$	$+2C^{\alpha}_{y}C^{\beta}_{z}$	$+4C^{\alpha}_{x}C'_{z}C^{\beta}_{z}$
Panel D	$-C^{\alpha}_{y}$	$+2C^{\alpha}_{x}C'_{z}$	$-2C^{\alpha}_{x}C^{\beta}_{z}$	$-4C^{\alpha}_{y}C'_{z}C^{\beta}_{z}$

If we associate with the above operators the following multiplet structures, these can explain the observed patterns reported in Fig. 2.

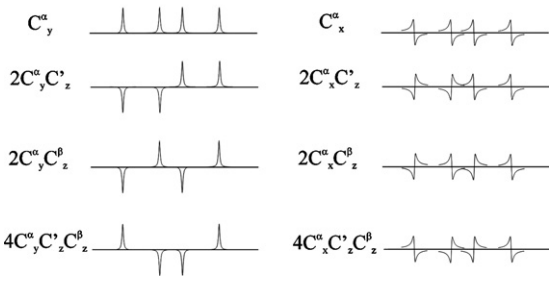

Therefore the expected patterns observed in the four experiments (A–D) are:

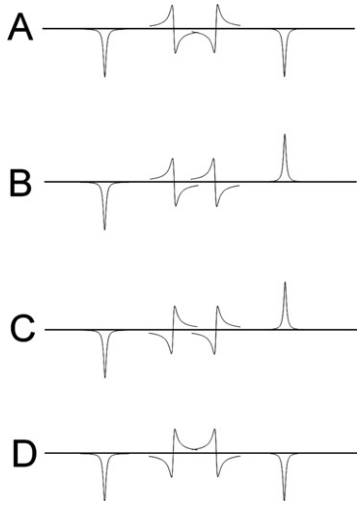

$+A + B + C + D$ yields the first (counting left to right) multiplet component (negative). $+A - B - C + D$ yields the fourth multiplet component (negative). $+A + B - C - D$ yields the second multiplet component, which needs to be phase corrected by 90° to be in the absoption mode. $+A - B + C - D$ yields the third multiplet component, which needs to be phase corrected by −90° to be in the absoption mode.

A.2. The S^3E building-block

Let's consider a spin system constituted by two spins, C^β, and C^α, where C^β is coupled to C^α, through $J_{C^\alpha C^\beta}$ and does not have any other large one-bond carbon–carbon couplings. The evolution of product operators at the different time points for the two different experiments reported hereafter is:

Panel A

(1) $-C^\beta{}_y$

$1 \rightarrow 3$

initial π_x pulse on C^α spin ($1 \rightarrow 2$); evolution of the C^α–C^β scalar coupling for $1/4J_{C^\alpha C^\beta}$, refocusing of C^β chemical shift (change is sign of the original $+C^\beta{}_y$ operator due to the central π_x pulse on C^β spin)

(3) $+C^\beta{}_y \cos(\pi J_{C^\beta C^\alpha} 2a) \; -2C^\beta{}_x C^\alpha{}_z \sin(\pi J_{C^\beta C^\alpha} 2a)$

$3 \rightarrow 4$ π_x pulse on C^β spin

(4) $-C^\beta{}_y \cos(\pi J_{C^\beta C^\alpha} 2a) \; -2C^\beta{}_x C^\alpha{}_z \sin(\pi J_{C^\beta C^\alpha} 2a)$

Panel B

(1) $+C^\beta{}_x$

$1 \rightarrow 2$ π_x pulse on C^β spin

(2) $+C^\beta{}_x$

$2 \rightarrow 4$

initial π_x pulse on C^α spin ($1 \rightarrow 2$); evolution of the C^α–C^β scalar coupling for $1/4J_{C^\alpha C^\beta}$, refocusing of C^β chemical shift (the sign of the original $+C^\beta{}_x$ operator due to the central π_x pulse on C^β spin does not change)

(4) $+C^\beta{}_x \cos(\pi J_{C^\beta C^\alpha} 2a) \; +2C^\beta{}_y C^\alpha{}_z \sin(\pi J_{C^\beta C^\alpha} 2a)$

Summarizing:

Panel A	$-C^\beta{}_y$	$-2C^\beta{}_x C^\alpha{}_z$
Panel B	$+C^\beta{}_x$	$+2C^\beta{}_y C^\alpha{}_z$

Therefore with the suitable linear combination of the two experiments, followed by a phase correction by 90° of one of the two, it is possible to separate the two multiplet components.

A.3. The C^α-NOESY-DS^3E pulse sequence

Narrow and wide carbon pulses correspond to $\pi/2$ and π pulses. Band-selective pulses are denoted by vertical shapes, hard pulses by rectangular symbols. Pulse field gradients (PFG line) are also indicated by shapes. All the gradients, used for purging and not for coherence selection, have a duration of 1.0 ms, and a sine-shape. The experimental parameters used are reported in the main text. The delays are: t_1 (the incremented delay in the indirect dimension), τ_m (mixing time), the delays a, b, c are set to satisfy the following relationships: $a + b + c = 1/4J_{C^\alpha C^\beta} = 7.2$ ms and $a - b + c = 1/4J_{C^\alpha C'} = 4.5$ ms. The phase cycle is: $\phi_1 = x, \; -x$; $\phi_2 = 4x, \quad 4(-x)$; $\phi_{DS^3E}(1) = 2x, 2(-x)$; $\phi_{DS^3E}(2) = 2y, 2(-y)$; $\phi_{DS^3E}(3) = 2(-y), 2y$; $\phi_{DS^3E}(4) = 2x, 2(-x)$; $\phi_{rec} = x, (-x), (-x), x, (-x), x, x, (-x)$. Quadrature detection in the F_1 dimension is obtained by incrementing ϕ_1 in a States-TPPI manner.

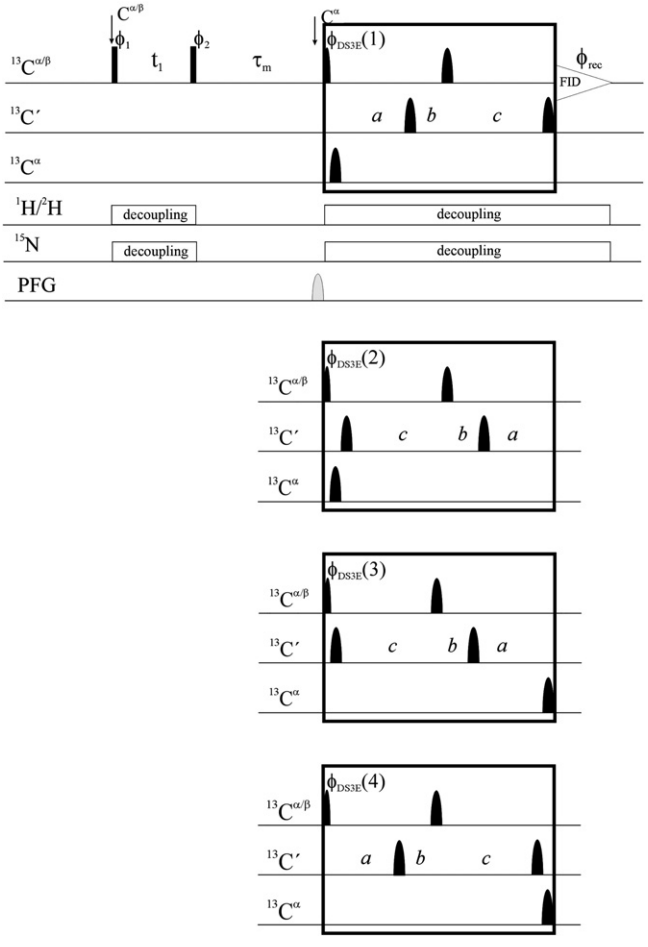

A.4. The Methyl-NOESY-S^3E pulse sequence

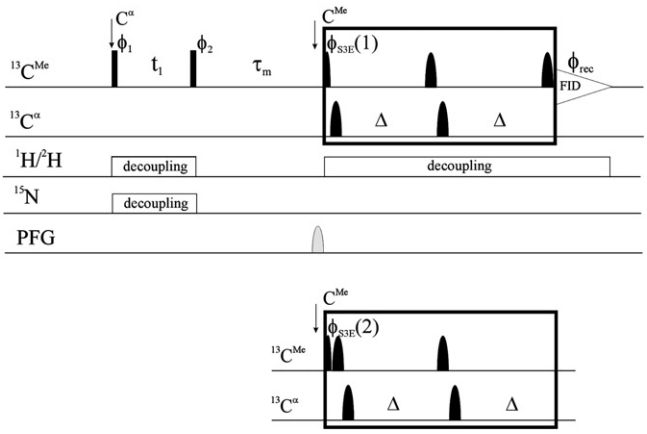

Narrow and wide carbon pulses correspond to $\pi/2$ and π pulses. Band-selective pulses are denoted by vertical shapes, hard pulses by rectangular symbols. Pulse field gradients (PFG line) are also indicated by shapes. All the gradients, used for purging and not for coherence selection, have a duration of 1.0 ms and a sine-shape. The experimental parameters used are reported in the main text. The delays are: t_1 (the incremented delay in the indirect dimension), τ_m (mixing time), the delay Δ is 3.6 ms. The phase cycle is: $\phi_1 = x, \quad -x; \quad \phi_2 = 4x, \quad 4(-x); \phi_{S^3E}(1) = 2x, 2(-x); \phi_{S^3E}(2) = 2y, 2(-y); \ \phi_{rec} = x, \ (-x), \ (-x), \ x, \ (-x), \ x, \ x, \ (-x)$. Quadrature detection in the F_1 dimension is obtained by incrementing ϕ_1 in a States-TPPI manner.

References

[1] I. Bertini, L. Duma, I.C. Felli, M. Fey, C. Luchinat, R. Pierattelli, P.R. Vasos, A heteronuclear direct detection NMR experiment for protein backbone assignment, Angew. Chem. Int. Ed. 43 (2004) 2257–2259.

[2] W. Bermel, I. Bertini, L. Duma, L. Emsley, I.C. Felli, R. Pierattelli, P.R. Vasos, Complete assignment of heteronuclear protein resonances by protonless NMR spectroscopy, Angew. Chem. Int. Ed. 44 (2005) 3089–3092.

[3] W. Bermel, I. Bertini, I.C. Felli, M. Piccioli, R. Pierattelli, ^{13}C-detected protonless NMR spectroscopy of proteins in solution, Progr. NMR Spectrosc. 48 (2006) 25–45.

[4] I. Bertini, I.C. Felli, L. Gonnelli, R. Pierattelli, Z. Spyranti, G.A. Spyroulias, Mapping protein–protein interaction by $^{13}C'$-detected heteronuclear NMR spectroscopy, J. Biomol. NMR 36 (2006) 111–122.

[5] W. Bermel, I. Bertini, I.C. Felli, Y.-M. Lee, C. Luchinat, R. Pierattelli, Protonless NMR experiments for sequence-specific assignment of backbone nuclei in unfolded proteins, J. Am. Chem. Soc. 128 (2006) 3918–3919.

[6] W. Bermel, I. Bertini, I.C. Felli, R. Kümmerle, R. Pierattelli, ^{13}C direct detection experiments on the paramagnetic oxidized monomeric copper, zinc superoxide dismutase, J. Am. Chem. Soc. 125 (2003) 16423–16429.

[7] B.-H. Oh, W.M. Westler, P. Darba, J.L. Markley, Protein carbon-13 spin systems by a single two-dimensional nuclear magnetic resonance experiment, Science 240 (1988) 908–911.

[8] U. Kolczak, J. Salgado, G. Siegal, M. Saraste, G.W. Canters, Paramagnetic NMR studies of blue and purple copper proteins, Biospectroscopy 5 (1999) S19–S32.

[9] I. Bertini, Y.-M. Lee, C. Luchinat, M. Piccioli, L. Poggi, Locating the metal ion in calcium-binding proteins by using cerium(III) as a probe, ChemBioChem 2 (2001) 550–558.

[10] T.E. Machonkin, W.M. Westler, J.L. Markley, ^{13}C–^{13}C 2D NMR: a novel strategy for the study of paramagnetic proteins with slow electronic relaxation times, J. Am. Chem. Soc. 124 (2002) 3204–3205.

[11] M. Kostic, S.S. Pochapsky, T.C. Pochapsky, Rapid recycle ^{13}C, ^{15}N and ^{13}C, ^{13}C heteronuclear and homonuclear multiple quantum coherence detection for resonance assignments in paramagnetic proteins: example of Ni^{2+}-containing acireductone dioxygenase, J. Am. Chem. Soc. 124 (2002) 9054–9055.

[12] F. Arnesano, L. Banci, I. Bertini, I.C. Felli, C. Luchinat, A.R. Thompsett, A strategy for the NMR characterization of type II copper(II) proteins: the case of the copper trafficking protein CopC from *Pseudomonas syringae*, J. Am. Chem. Soc. 125 (2003) 7200–7208.

[13] A. Eletsky, O. Moreira, H. Kovacs, K. Pervushin, A novel strategy for the assignment of side-chain resonances in completely deuterated large proteins using (13)C spectroscopy, J. Biomol. NMR 26 (2003) 167–179.

[14] K. Pervushin, A. Eletsky, A new strategy for backbone resonance assignment in large proteins using a MQ-HACACO experiment, J. Biomol. NMR 25 (2003) 147–152.

[15] Z. Serber, C. Richter, D. Moskau, J.-M. Boehlen, T. Gerfin, D. Marek, M. Haeberli, L. Baselgia, F. Laukien, A.S. Stern, J.C. Hoch, V. Dötsch, New carbon-detected protein NMR experiments using cryoprobes, J. Am. Chem. Soc. 122 (2000) 3554–3555.

[16] A. Meissner, J.O. Duus, O.W. Sørensen, Spin-state-selective excitation. Application for E.COSY-type measurement of J(HH) coupling constants, J. Magn. Reson. 128 (1997) 92–97.

[17] M.D. Sørensen, A. Meissner, O.W. Sørensen, Spin-state-selective coherence transfer via intermediate states of two-spin coherence in IS spin systems: application to E.COSY-type measurement of J coupling constants, J. Biomol. NMR 10 (1997) 181–186.

[18] M. Ottiger, F. Delaglio, A. Bax, Measurement of J and dipolar couplings from simplified two-dimensional NMR spectra, J. Magn. Reson. 131 (1998) 373–378.

[19] P. Andersson, J. Weigelt, G. Otting, Spin-state selection filters for the measurement of heteronuclear one-bond coupling constants, J. Biomol. NMR 12 (1998) 435–441.

[20] B. Brutscher, Accurate measurement of small spin–spin couplings in partially aligned molecules using a novel J-mismatch compensated spin-state-selection filter, J. Magn. Reson. 151 (2001) 332–338.

[21] L. Duma, S. Hediger, B. Brutscher, A. Bockmann, L. Emsley, Resolution enhancement in multidimensional solid-state NMR spectroscopy of proteins using spin-state selection, J. Am. Chem. Soc. 125 (2003) 11816–11817.

[22] L. Duma, S. Hediger, A. Lesage, L. Emsley, Spin-state selection in solid-state NMR, J. Magn. Reson. 164 (2003) 187–195.

[23] R. Verel, T. Manolikas, A.B. Siemer, B.H. Meier, Improved resolution in (13)C solid-state spectra through spin-state-selection, J. Magn. Reson. 184 (2007) 322–329.

[24] A. Meissner, J.O. Duus, O.W. Sørensen, Integration of spin-state-selective excitation into 2D NMR correlation experiments with the heteronuclear ZQ/2Q pi rotations for 1JXH- resolved E.COSY-type measurements of heteronuclear coupling constants in proteins, J. Magn. Reson. 128 (1997) 92–97.

[25] L. Banci, M. Benedetto, I. Bertini, R. Del Conte, M. Piccioli, T. Richert, M.S. Viezzoli, Assignment of backbone NMR resonances and secondary structural elements of a reduced monomeric mutant of copper/zinc superoxide dismutase, Magn. Reson. Chem. 35 (1997) 845–853.

[26] M. Matzapetakis, P. Turano, E.C. Theil, I. Bertini, ^{13}C–^{13}C NOESY spectra of a 480 kDa protein: solution NMR of ferritin, J. Biomol. NMR 38 (2007) 237–242.

[27] A.J. Shaka, J. Keeler, R. Freeman, Evaluation of a new broadband decoupling sequence: WALTZ-16, J. Magn. Reson. 53 (1983) 313–340.
[28] A.J. Shaka, P.B. Barker, R. Freeman, Computer-optimized decoupling scheme for wideband applications and low-level operation, J. Magn. Reson. 64 (1985) 547–552.
[29] L. Emsley, G. Bodenhausen, Gaussian pulse cascades: new analytical functions for rectangular selective inversion and in-phase excitation in NMR, Chem. Phys. Lett. 165 (1990) 469–476.
[30] M. Kadkhodaie, O. Rivas, M. Tan, A. Mohebbi, A.J. Shaka, Broadband homonuclear cross polarization using flip-flop spectroscopy, J. Magn. Reson. 91 (1991) 437–443.
[31] I. Bertini, I.C. Felli, R. Kümmerle, C. Luchinat, R. Pierattelli, ^{13}C–^{13}C NOESY: a constructive use of ^{13}C–^{13}C spin-diffusion, J. Biomol. NMR 30 (2004) 245–251.
[32] W. Bermel, I. Bertini, I.C. Felli, R. Kümmerle, R. Pierattelli, Novel ^{13}C direct detection experiments, including extension to the third dimension, to perform the complete assignment of proteins, J. Magn. Reson. 178 (2006) 56–64.
[33] L. Banci, I. Bertini, C.Y. Chiu, G.T. Mullenbach, M.S. Viezzoli, Synthesis and characterization of a monomeric mutein of Cu/Zn superoxide dismutase with partially reconstituted enzymatic activity, Eur. J. Biochem. 234 (1995) 855–860.
[34] I. Bertini, I.C. Felli, R. Kümmerle, D. Moskau, R. Pierattelli, ^{13}C–^{13}C NOESY: an attractive alternative to study large macromolecules, J. Am. Chem. Soc. 126 (2004) 464–465.
[35] M.W.F. Fischer, L. Zeng, E.R.P. Zuiderweg, Use of ^{13}C–^{13}C NOE for the assignmetn of NMR lines of larger labeled proteins at larger magnetic fields, J. Am. Chem. Soc. 118 (1996) 12457–12458.
[36] N.K. Goto, K.H. Gardner, G.A. Mueller, R.C. Willis, L.E. Kay, A robust and cost-effective method for the production of Val, Leu, Ile (delta 1) methyl-protonated ^{15}N-, ^{13}C-, ^{2}H-labeled proteins, J Biomol NMR 13 (1999) 369–374.